Static and Dynamic Properties of Adsorbed Chains at Surfaces: Monte Carlo Simulation of a Bead-Spring Model

Andrey Milchev† and Kurt Binder*

Institut für Physik, Johannes-Gutenberg-Universität Mainz, D-55099 Mainz, Staudinger Weg 7, Germany

Received May 16, 1995; Revised Manuscript Received September 22, 1995⊗

ABSTRACT: The adsorption of flexible polymers from dilute solution in good solvents at attractive walls is studied by Monte Carlo simulation of a coarse-grained off-lattice model, varying chain length N and the strength ϵ of a short-range attractive wall potential. Unlike many previous studies, no chain end (or other monomer) is held fixed near the wall. In qualitative agreement with previous work on different models, we find an adsorption transition at a critical strength of the wall potential, where the chain configuration changes from three-dimensional to quasi-two-dimensional in the limit of very long chains. The dynamics of the chains is studied both above and below this adsorption threshold ϵ_c. Time-dependent mean-square displacements of monomers and the chain center of gravity as well as the associated relaxation times are studied in detail. In the adsorbed phase, relaxation times are found to scale as $\tau \propto N^{z_{\text{eff}}}$ with $z_{\text{eff}} \approx 2.65 \pm 0.1$ and the lateral diffusion constant scales as $D_N \propto N^{-y_{\text{eff}}}$ with $y_{\text{eff}} \approx 1.1$. Also small-scale motions of monomers in different distances from the adsorbing wall are investigated, and a qualitative picture for the dynamics of these partially adsorbed chains is developed.

1. Introduction

Polymer chains at free surfaces or interfaces between materials find much recent interest today, both because they pose challenging problems to fundamental research and because of applications in technology and biology (adsorption of biopolymers at cell membranes, etc.).[1−5] While the static aspects of the adsorption of single chains at walls have been studied for a long time (see, e.g., ref 5 for a review), the dynamic properties of polymers adsorbed on surfaces have received much less attention.[6,7] Most work considers either the kinetics of the adsorption or desorption of polymers at a solid surface[6] or the collective dynamics of an adsorbed layer of many chains,[7] while the dynamics of single chains that are adsorbed on walls are considered only occasionally.[8−12] Note that we do not address here chains with special grafting end groups forming "polymer brushes",[13−16] which recently have found a lot of attention, but rather address chains whose ends are attracted to the wall in the same way as inner monomers. We focus here on the behavior of single chains, in the situation where the wall is exposed to a dilute polymer solution in the good solvent case, rather than considering thin films of bulk polymeric material in contact with walls.[1−4,17−20]

Clearly, this problem is not easy to address neither by experiment[4,6,7] nor from the point of view of analytical theory,[21,22] and thus computer simulation is the method of choice here. Previous work has mostly been concerned with the relaxation of strongly adsorbed chains near the glass transition of such chains,[9−12] resulting from the fact that diffusion over long distances requires concerted motion at the many points where the chain is attached to the surface,[6] and the monomer density at this surface may be rather high.[8]

In the present paper, we wish to avoid the difficulties associated with the glass transition (relaxation times easily reach astronomical values on the microscopic time scales of computer simulations, which then are correspondingly difficult[23,24]). We focus on *weakly adsorbed* chains, where the length of the "trains"[3] (sequences of adsorbed monomers attached to the wall) is still small enough, such that the fraction of monomers in "loops" or "tails" is still large and the concentration in the region immediately adjacent to the wall is at most semidilute. Note that "weakly adsorbed" in the sense defined above does not mean that the adsorption energy per monomer $|\epsilon|$ is small in comparison to k_BT, since important entropic effects occur: rather weakly adsorbed means $|\epsilon - \epsilon_c| \ll |\epsilon_c|$, $|\epsilon_c|$ being the adsorption energy at threshold.[5] We wish to clarify the dynamical properties of the chains in this regime as a function of chain length and the strength of wall−monomer interaction. The latter controls the fraction of adsorbed monomers in the trains, of course. Loops and tails, however, extend in the third dimension, and thus it is questionable to what extent the chain moves as a strictly two-dimensional object.

In section 2, we summarize briefly the model and simulation technique: We use an off-lattice bead-spring model that has proven efficient and useful for the study of static and dynamic properties of chains in dilute and concentrated polymer solutions in the bulk.[25−27] Unlike lattice models,[28,29] this model should not suffer from ergodicity problems in the presence of geometrical constraints,[25,30] and it has been used already successfully for modeling chain motion in pores with attractive walls.[30] In section 3, we briefly summarize the static properties of a chain in the presence of an attractive wall, for our model. Of course, static properties of the adsorption transition and its universal aspects in the scaling limit[5,31] can be studied for lattice models by various techniques more precisely,[32−35] but this is not our primary interest here, where we only clarify the static properties of the model as a prerequisite to an analysis of the dynamical behavior. Section 4 discusses the dynamical properties of the chains for variable strength of the attractive interaction with the wall; both nonadsorbed chains and adsorbed ones are considered. Section 5 then summarizes our conclusions. Results of the related problem of the dynamics of chains in a quasi-two-dimensional geometry enforced not by attraction to a single wall (in a semi-infinite geometry) but by

† Present and permanent address: Institute of Physical Chemistry, Bulgarian Academy of Sciences, 1040 Sofia, Bulgaria.

⊗ Abstract published in *Advance ACS Abstracts,* November 15, 1995.

0024-9297/96/2229-0343$12.00/0

confinement between two walls (i.e., a slitlike pore) are described in a separate paper.

Unlike some work with lattice models,[36] we assume an ideal flat surface without any heterogeneity. Thus, our chains are free to move laterally on the surface; without energy cost a chain could be displaced as a whole. At this point, the model certainly is too idealized to describe experiments (real surfaces exhibit corrugation, large-scale roughness, and other defects; also hydrodynamic interactions are present). But the model is very suitable for testing the theoretical questions, and it is a suitable starting point for more refined models that take more complications of real systems into account.

2. Comments on the Model and the Simulation Technique

We are not aiming at the explanation of the properties of particular polymers (such as polyethylene, polypropylene, polycarbonate, etc.), but rather we wish to contribute to the general understanding of universal properties of flexible polymers. Thus, we choose a coarse-grained model, where a chain consists of coarse-grained monomers connected by coarse-grained bonds (each bond representing at least $n \approx 3-6$ chemical bonds along the backbone of a polymer chain). Each coarse-grained bond is described by the so-called FENE potential (finitely extensible nonlinear elastic potential) where a bond l has a maximum length l_{max}

$$U_{FENE}(l) = -K(l_{max} - l_0)^2 \ln\left[1 - \left(\frac{l - l_0}{l_{max} - l_0}\right)^2\right] \quad (1)$$

Obviously the minimum of this potential occurs for $l = l_0$, $U_{FENE}(l_0) = 0$, near l_0 it is harmonic, with K being a spring constant, and the potential diverges to infinity both when $l \rightarrow l_{max}$ and when $l \rightarrow l_{min} = 2l_0 - l_{max}$, and choosing our length unit $l_{max} = 1$, we choose the other parameters as[27]

$$l_{min} = 0.4, \quad l_0 = 0.7, \quad K/k_BT = 20 \quad (2)$$

T being the absolute temperature and k_B Boltzmann's constant. We treat our chains as fully flexible, and, thus, we do not include a potential for bond angles (although this can be added straightforwardly for a description of semiflexible chains[37]).

The nonbonded interaction between effective monomers is described by a Morse-type potential, r being the distance between the beads representing the effective monomeric units,[26,30]

$$U_M(r)/\epsilon_M = \exp[-2\alpha(r - r_{min})] - 2\exp[-\alpha(r - r_{min})] \quad (3)$$

with parameters $\epsilon_M/k_BT = 0.1$, $\alpha = 24$, and $r_{min} = 0.8$. As shown in previous work,[26] the decay of this potential with distance r is so rapid that $U_M(r) \approx 0$ for $r > 1$ with negligible error; this allows the use of a link-cell algorithm with a cell linear dimension of unity and leads to a reasonably fast performance of our Monte Carlo program.

We choose units such that $k_B \equiv 1$ and $\epsilon_M = 0.1$. Then the Θ temperature,[40] where a single coil of N effective monomeric units in dilute solution in the bulk behaves for $N \rightarrow \infty$ as a Gaussian coil, is $\Theta \approx 0.62$.[27] Our temperature $T = 1$ hence implies $T \gg \Theta$; i.e., we work under good solvent conditions.

As an adsorption geometry, we consider a semi-infinite system with an impenetrable wall at $z = 0$, such that monomer positions are restricted to the positive half-space $z > 0$. Following our previous study of chain motions in straight tubes,[30] we choose a square well attractive potential at the wall

$$U_W(z) = \epsilon, \quad z \le \delta; \qquad U_W(z) = 0, \; z > \delta \quad (4)$$

Our simulations have been carried out for a wide range of the strength of this attractive potential, ϵ/k_BT, and of chain length N ($16 \le N \le 128$). The potential range has been fixed at $\delta = 1/8$, i.e., a value much smaller than the length of effective bonds. This is physically reasonable, since each effective bond represents a sequence of several chemical monomers. As will be shown in the following section, this model then shows an adsorption transition where chain configurations change from three-dimensional to quasi-two-dimensional,[5,32-35] at about $\epsilon_c/k_BT \approx -1.90 \pm 0.05$. Figure 1 shows typical snapshot pictures of our chains for a weakly adsorbed case ($\epsilon/k_BT = -2.5$) and a more strongly adsorbed case ($\epsilon/k_BT = -3.0$).

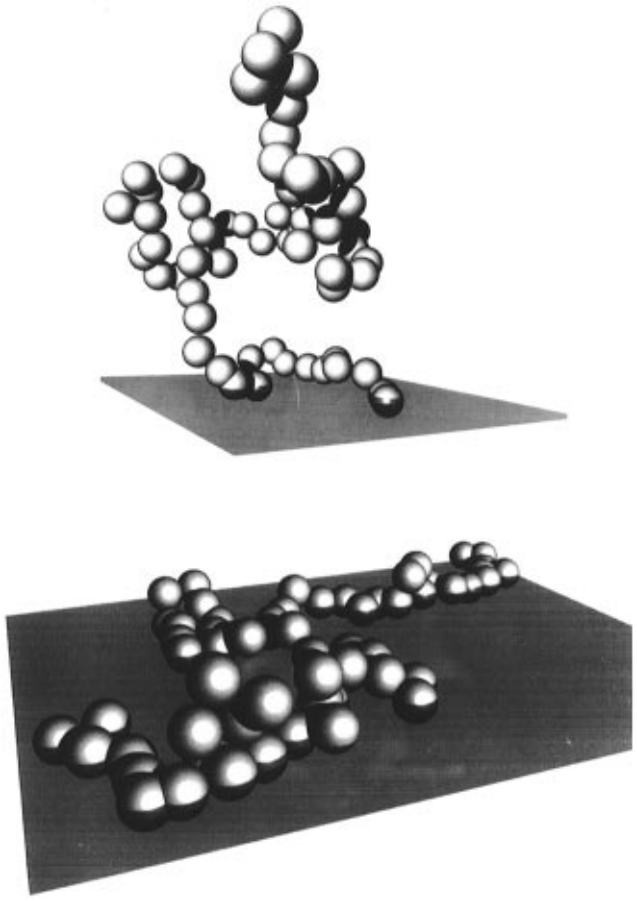

Figure 1. Snapshot picture of a bead-spring chain containing $N = 64$ effective monomeric units at $\epsilon/k_BT = -2.5$ (a, top) and at $\epsilon/k_BT = -3.0$ (b, bottom). The adsorbing plane $z = 0$ is shown shaded. Effective monomers are represented as spheres of radius $l_{min} = 0.4$, while the bonds between the effective monomers are not shown. Note that there is a short range repulsion between effective monomers due to the Morse-potential (eq 3), but there is no repulsion between the monomers and the wall as long as $z > 0$, while no monomer can cross the plane $z = 0$ since $U_w(z < 0) = \infty$.

Of course, such a choice of wall potential as used here leads to certain peculiarities at short distances near the wall, as one can see in the monomer density profile $n(z)$, for instance (Figure 2). The step of the potential at $z = \delta$ leads to a kink in this density profile. If we choose a much larger range of the potential, e.g., $\delta = 1$ (Figure 2), this singular behavior at $z = \delta$ is much less

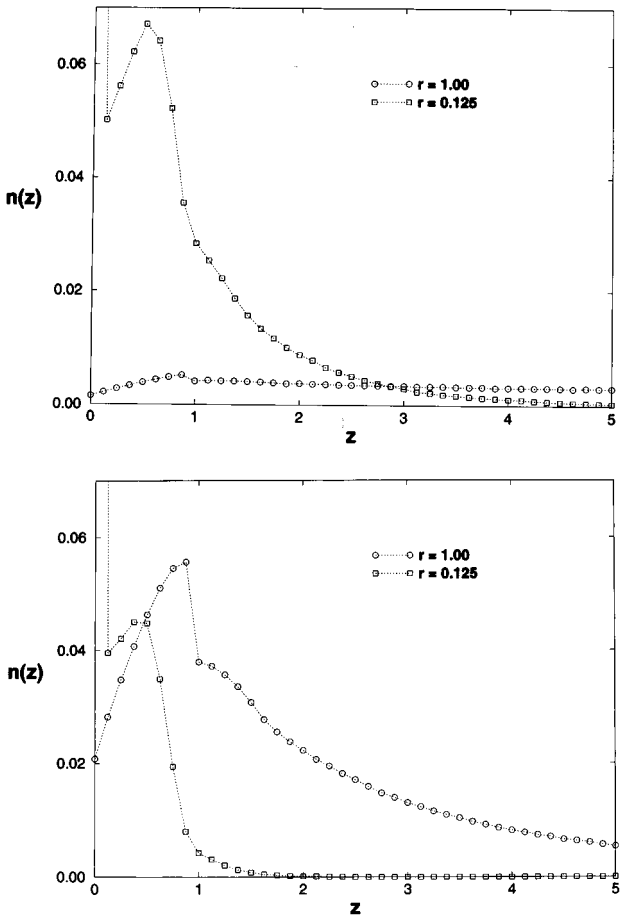

Figure 2. Plot of the monomer density $n(z)$ versus z for chain length $N = 128$, in a weakly adsorbed case (a, top) $\epsilon/k_BT = -2.50$, and in a strongly adsorbed case (b, bottom), $\epsilon/k_BT = -3.00$. Squares refer to a potential range of $\delta = 1/8$ in both cases, while circles refer to the choice $\delta = 1$ and $\epsilon/k_BT = -0.268\ 75$ (a) and $\epsilon/k_BT = -0.375$ (b).

pronounced. Of course, there is a nontrivial renormalization of the scale of the potential strength ϵ/k_BT if δ is varied, but on scales $z \gg \delta$ we expect a qualitatively similar behavior, if one works at the proper values of ϵ/k_BT in both cases (note that the actual form of the profiles in Figure 2 already shows that for $\delta = 1$ both choices of ϵ are clearly in the nonadsorbing state of the surface. While for gaussian chains this correspondence simply follows from requiring[5,38] that $\epsilon\delta^2/k_BT =$ constant, for chains in the excluded volume regime the proper rescaling of ϵ/k_BT is nontrivial). On a scale $z \approx \delta$, no universal behavior at all is to be expected. Being interested here in the universal aspects of the adsorption behavior, it is advisable to work with a small value of δ, and hence only the choice $\delta = 1/8$ will be considered further in the following.

As described in previous work,[25−27,30] this model can be simulated fairly efficiently with a dynamic Monte Carlo algorithm. The attempted Monte Carlo update involves choosing a monomeric unit at random and attempting to displace it randomly by displacements Δx, Δy, Δz chosen uniformly from the intervals $-0.5 \le \Delta x$, Δy, $\Delta z \le +0.5$. From the total change ΔU of the potential energies defined above, the transition probability Ω is calculated as usual,[28]

$$\Omega = \min\{\exp[-\Delta U/(k_BT)], 1\} \qquad (5)$$

This attempted move is accepted only if Ω exceeds a random number η, uniformly distributed in the interval

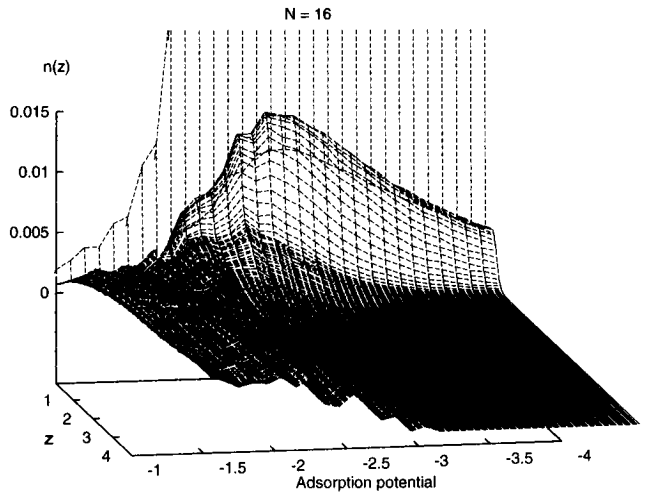

Figure 3. Density $n(z)$ plotted as function of distance z from the adsorbing wall and as a function of the strength ϵ/k_BT of the wall potential, for chain length $N = 16$. Vertical dotted lines denote the density of the monomers, "sticking" immediately at the wall; for $|\epsilon/k_BT| > 2.0$ this density exceeds rapidly the value $n(z) = 0.015$, which still lies within the figure's border.

$0 \le \eta < 1$. Note that the potentials eqs 1−3 are constructed such that chains cannot intersect themselves in the course of random displacements of beads.[25−27] Thus, unlike early off-lattice Monte Carlo work,[39] one does not need to check separately for entanglement restrictions. Thus, our algorithm is rather fast; between 2.5×10^4 and 6×10^4 attempted updates of monomeric units per CPU second are performed on simple RISC workstations such as IBM RS 6000/370. The precise value of the speed depends on the acceptance rate of the attempted moves and thus on the thermodynamic conditions.

The data of the present paper were then generated by carrying out about 200 runs at each state point (N; ϵ/k_BT), where each run was propagated to a length of about 2×10^6 attempted Monte Carlo steps (MCS) per monomer (1 MCS will be our unit of "time" in the following). So, many independent runs are necessary in order to reach a reasonable statistical accuracy.

3. Static Properties of Chains Adsorbed at Flat Walls

In order to get an overview of where the adsorption transition occurs, it is convenient to study the density profile $n(z)$ as a function of the strength of the adsorption potential (Figures 3 and 4). In all cases there is a strong density enhancement in the regime $0 < z < \delta = 1/8$, due to the monomers which win adsorption energy at the wall. In the nonadsorbed case ($|\epsilon/k_BT| < |\epsilon_c/k_BT|$), the density has then only a very mild second maximum near $z \approx 0.7$, while then $n(z)$ develops to a flat plateau, $n(z \gg 1) = n_0$, the density of the bulk solution. Of course, since we cannot simulate a truly infinite or semi-infinite system, we have to choose a finite extension in the $+z$-direction, placing a second (purely repulsive) wall at $z = D = 16$; in addition, we choose finite linear dimensions L in the x,y-directions parallel to the wall, applying periodic boundary conditions in these parallel directions. If the distribution of the monomers of a chain in this geometry would be uniform, it would simply be given by $n_0 = N/(L^2D)$. Choosing $L = 32$ for $N = 64$ would yield $n_0 = 1/256$. Due to the adsorption potential, $n(z)$ is enhanced over this value even for $z = 3-4$ still by a factor of about 2. However, when the chain gets adsorbed ($|\epsilon/k_BT| > |\epsilon_c/k_BT|$), the density

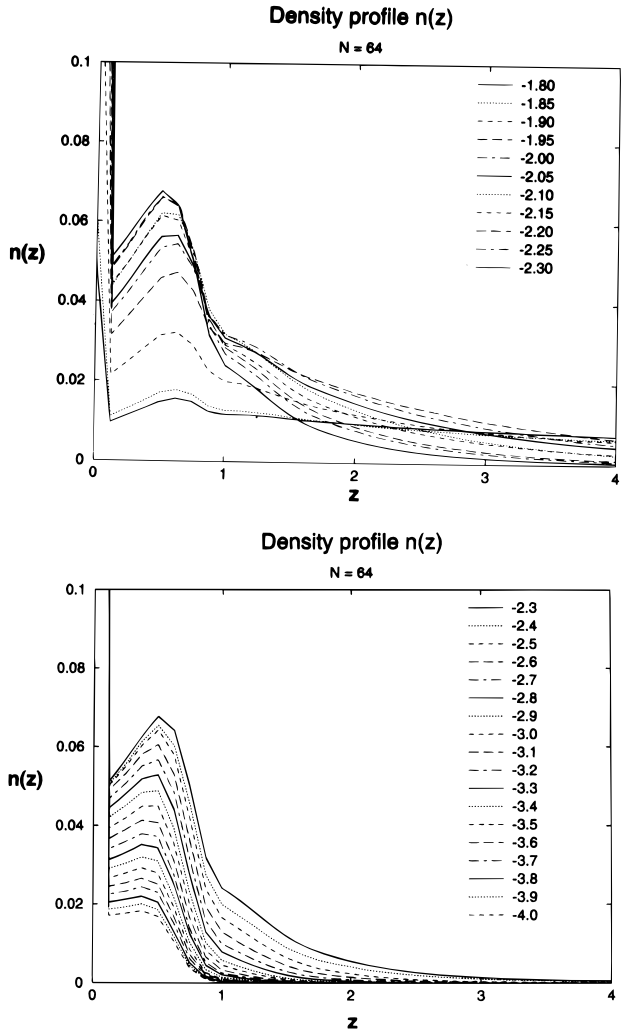

Figure 4. Density profile $n(z)$ plotted versus z for $N = 64$ for various values ϵ/k_BT of the strength of the wall potential, from $\epsilon/k_BT = -1.80$ to -2.30 (a, top) and from $\epsilon/k_BT = -2.30$ to -4.0 (b, bottom). Note that in the latter case the order of the curves is from above to below, while in the former case near $z \approx 0.5$ $\epsilon/k_BT = -1.80$ is the curve closest to the bottom and $\epsilon/k_BT = -2.3$ is the curve closest to the top. The curves are just cross sections through the perspective global view presented in Figure 3.

profile develops a pronounced peak near $z \approx 0.5$ to $z \approx 0.7$, and $n(z)$ decays essentially to zero for large z. This peak of $n(z)$ that is seen for $z \approx 0.5-0.7$ for all values of ϵ is basically due to such nonadsorbed monomers which are nearest neighbors of adsorbed monomers along the chain. Since we always consider $|\epsilon/k_BT| > 1$, the density of monomers adsorbed at the wall always is enhanced in comparison to n_0, and also the density of nonadsorbed nearest neighbors (along the chain) of such adsorbed monomers is enhanced. While for choices of $|\epsilon|$ that exceed the threshold value $|\epsilon_c|$ for adsorption only slightly, the trains of neighboring adsorbed monomers are still rather short, and the loops of nonadsorbed monomers between neighboring trains are relatively large; this is not true in the strongly adsorbed case ($|\epsilon| \gg |\epsilon_c|$). Then, the peak near $z \approx 0.5$ to $z \approx 0.7$ decreases in height with increasing strength $|\epsilon|$ of the wall potential because more and more monomers become part of trains rather than being part of "loops" or "tails". Then, $n(z)$ for $z \gtrsim 1$ is already essentially zero.

As expected, this qualitative picture of the adsorption transition is in full accord with the standard theoretical concepts on this problem.[3-5] Apart from the density profile, the transition shows up in many other characteristics: the fraction f_a of adsorbed bonds (Figure 5a), the total internal energy E (Figure 5b), and the average orientation of bonds, measured by the second Legendre polynomial $P_2(\cos\theta)$ (Figure 5c)

$$P_2(\cos\theta) = {}^1/_2(3\langle\cos^2\theta\rangle - 1) \qquad (6)$$

where θ measures the angle between an effective bond and the z-axis, and the average is taken over by all configurations of the polymer and all its effective bonds. Since $P_2(\cos\theta) = 1$ if all bonds were oriented perpendicular to the surface, $P_2(\cos\theta) = -{}^1/_2$ if they are oriented parallel to the surface, while $P_2(\cos\theta) = 0$ for random orientation, the behavior seen in Figure 5c is easily interpreted: a random orientation occurs in the nonadsorbed phase, for $|\epsilon| < |\epsilon_c|$, while in the adsorbed phase more and more bonds become aligned parallel to the wall, as the effective monomers connected by the bond both become part of a train adsorbed at the wall. Thus, either f_a or $P_2(\cos\theta)$ behave like an "order parameter" of the adsorption transition and for $\epsilon = -4$ are already close to their saturation values ($f_A = 1$ or $P_2(\cos\theta) = -{}^1/_2$, respectively). Of course, this transition is a sharp transition only in the limit of infinite chain length.[5,32] From Figure 5a–c, we conclude that in our model this transition occurs at $\epsilon_c = -1.90 \pm 0.05$. (Remember units are chosen such that $k_BT = 1$ here.)

It is also interesting to note that local quantities like the mean-square bond length $\langle l^2\rangle$ (Figure 5d) reflect this transition too. This effect results since for a free chain the FENE-potential eq 1 refers to a problem of an (anharmonic) oscillator with 3 degrees of freedom, namely, the three Cartesian components of a displacement vector, while for a strongly adsorbed chain effectively only two components remain, namely, displacement parallel to the wall. This suppression of 1 degree of freedom induces the decrease seen in $\langle l^2\rangle$ for $|\epsilon| > |\epsilon_c|$.

According to the scaling theory of the adsorption transition[5,32] one expects for ϵ near ϵ_c in the limit $N \to \infty$ a power law behavior,

$$f_a \propto -P_2(\cos\theta) \propto (\epsilon/\epsilon_c - 1)^{(1/\phi)-1}, \quad \epsilon \to \epsilon_c \qquad (7)$$

where the so-called crossover exponent ϕ has been estimated from early Monte Carlo work[32] as $\phi \approx 0.58$, while second-order renormalization group expansions[40] implied $\phi \approx 0.67$. Figure 6 provides a check of eq 7. Note that $\phi = 0.58$ would imply a slope of 0.72 for both quantities displayed in Figure 6. The fact that both quantities do not exhibit precisely the same slope on the log–log plot indicates that the asymptotic region near ϵ_c, where eq 7 is supposed to hold, has not really been reached, and the slopes seen in Figure 6 are "effective exponents" only. However, we cannot analyze data for ϵ nearer to ϵ_c here, since the chain length $N = 128$ then already exhibits pronounced rounding of the transition, and significantly longer chains would be required for accurate estimates.[29,33,34] Thus, it also is not straightforward to estimate the critical value ϵ_c itself with better precision. Actually Figure 6 is not meant as a precise estimation of critical exponents but rather as a demonstration that our data are roughly compatible with the expected behavior.

The adsorption transition also shows up in the behavior of the chain linear dimensions. Figure 7a shows the mean-square gyration radii, distinguishing parallel ($\langle R_{g\parallel}^2\rangle$) and perpendicular ($\langle R_{g\perp}^2\rangle$) components. While these components in the z-direction normal to the surface and in an x- or y-direction parallel to the surface do not differ from each other for $|\epsilon| \ll |\epsilon_c|$, for $|\epsilon| > |\epsilon_c|$

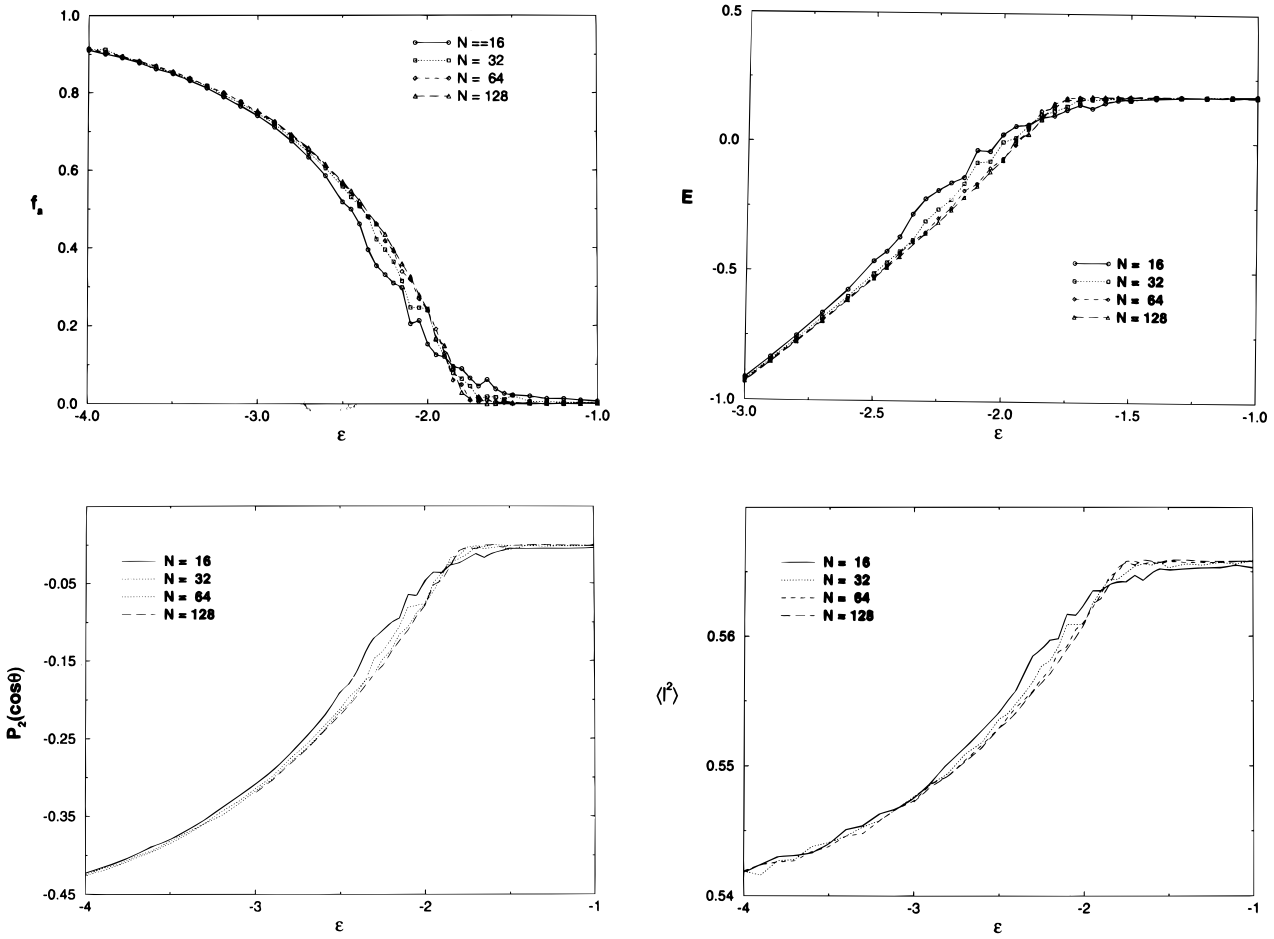

Figure 5. (a, top left) Fraction f_a of adsorbed monomers (i.e., monomers having a z-coordinate less than δ) plotted vs ϵ/k_BT (choosing units such that $k_BT \equiv 1$). Four different symbols denote chain lengths $N = 16$, 32, 64, and 128, as indicated. (b, top right) Total internal energy per monomer E plotted vs ϵ. (c, bottom left) Second Legendre polynomial $P_2(\cos\theta)$ plotted vs ϵ. Four types of curves show different chain lengths $N = 16$, 32, 64, and 128. (d, bottom right) Mean-square length $\langle l^2 \rangle$ plotted vs ϵ.

the parallel component strongly increases, while the perpendicular component decreases.

When we analyze this behavior for different chain lengths (Figure 7b,c), we see that for $|\epsilon| < |\epsilon_c|$ the chains scale with N in the same way as they do in dilute solution in good solvent in the bulk,

$$\langle R_{g_\parallel}{}^2 \rangle \propto \langle R_{g_\perp}{}^2 \rangle \propto \langle R_g{}^2 \rangle_{\text{bulk}} \propto N^{2\nu}, \quad \nu \approx 0.59 \qquad (8)$$

In contrast, for $|\epsilon| > |\epsilon_c|$ one sees that $\langle R_{g_\perp}{}^2 \rangle / N^{2\nu} \to 0$ for $N \to \infty$: this happens because the thickness of the adsorbed chain is finite; it is controlled by the distance $|\epsilon - \epsilon_c|$ from the adsorption threshold, but does not diverge as $N \to \infty$. At the same time, we see a steady increase of $\langle R_{g_\parallel}{}^2 \rangle / N^{2\nu}$ with increasing chain length (Figure 7c): This happens because the adsorbed chain follows the two-dimensional self-avoiding walk statistics, with an exponent $\nu_2 = {}^3/_4$.[31,32]

$$\langle R_{g_\parallel}{}^2 \rangle \propto N^{2\nu_2}, \quad |\epsilon| > |\epsilon_c| \qquad (9)$$

Since in the regime of ϵ shown the chains rearrange their configurations via a rather slow relaxation, as will be analyzed in the next section, the statistical accuracy of these data obviously is not very good. And while the data are roughly compatible with a crossover scaling description as suggested by Eisenriegler et al.,[32] we clearly are unable to present precise estimates of crossover scaling functions (Figure 8). Note, however, that in the present work we do not suppress fluctuations by fixing one chain end at the wall, as done in ref

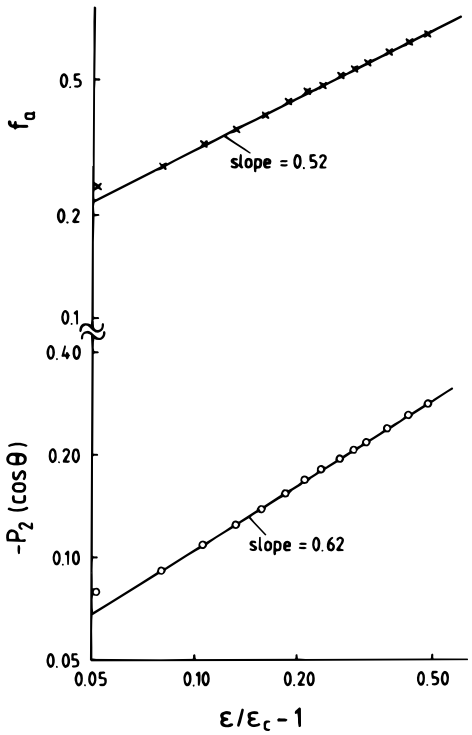

Figure 6. log−log plot of the fraction f_a of adsorbed monomers (upper part) and of the orientational order parameter $-P_2(\cos\theta)$ (lower part) versus the distance from the adsorption threshold, using $\epsilon_c = -1.9$ and plotting data for the longest chain length $N = 128$ only.

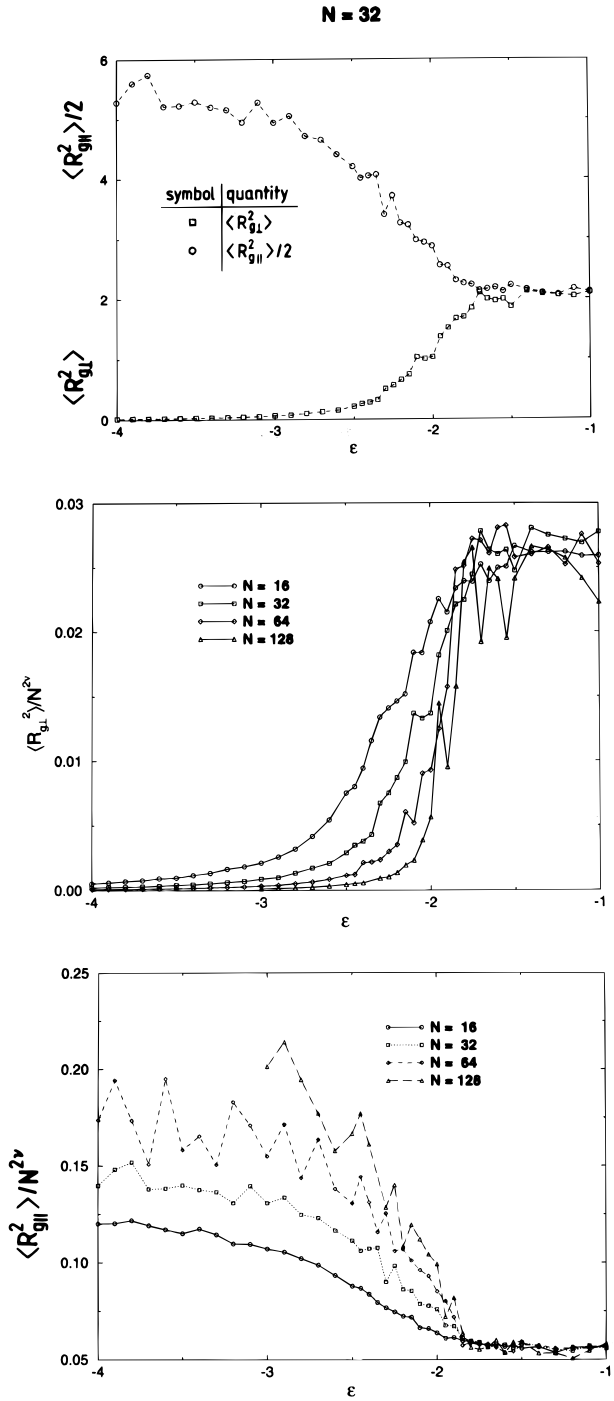

Figure 7. (a, top) Perpendicular component ($\langle R_{g_\perp}{}^2 \rangle$) of the mean-square gyration radius and a parallel component $\{\langle R_{g_\parallel}{}^2 \rangle/2 = (\langle R_{gx}{}^2 \rangle + \langle R_{gy}{}^2 \rangle)/2\}$ plotted vs ϵ for $N = 32$. (b, middle) Perpendicular component of the mean-square gyration radius normalized by a factor $N^{2\nu}$ where $\nu = 0.59$ is the exponent characterizing the coil size in the good solvent regime,[29,31] plotted vs ϵ for four different chain lengths. (c, bottom) Same as b but for the parallel component.

32; the latter work also used simple sampling techniques for lattice chains and hence was completely unable to yield any information on the dynamics of adsorbed chains, unlike the present work.

If we would fix a chain end at the wall, we would constrain the configuration of the chain even in the nonadsorbed phase for $|\epsilon| < |\epsilon_c|$. Then, a systematic deviation between $\langle R_{g_\parallel}{}^2 \rangle/2$ and $\langle R_{g_\perp}{}^2 \rangle$ would occur for all ϵ. Such a distinction also occurs if we constrain the center of mass position Z_{CM} of a chain at a distance close to the wall (Figure 9). Such a distinction, however, does

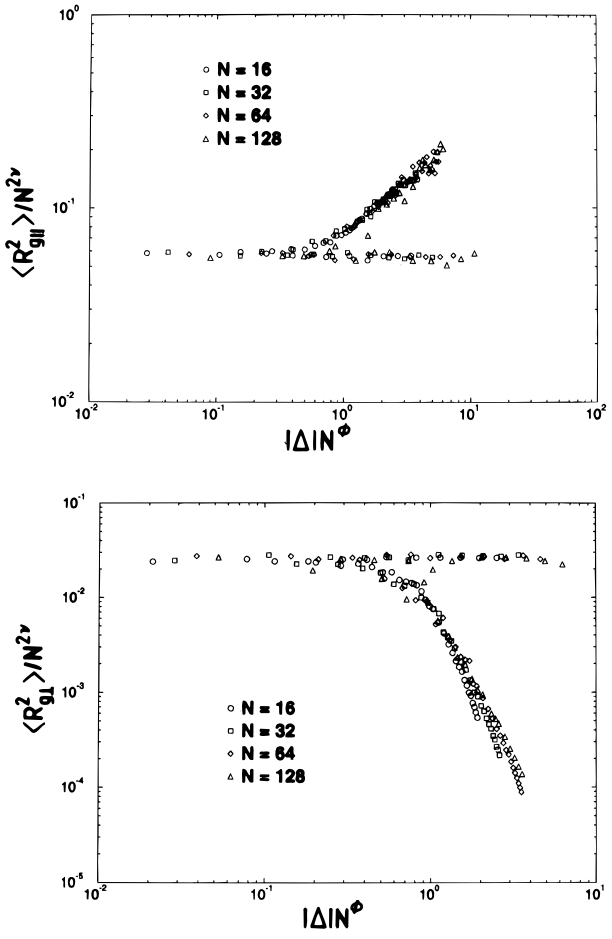

Figure 8. Crossover scaling description of the parallel ($\langle R_{g_\parallel}{}^2 \rangle$) and perpendicular ($\langle R_{g_\perp}{}^2 \rangle$) components of the mean-square gyration radius, plotting $\langle R_{g\parallel}{}^2 \rangle / N^{2\nu}$ (a, top) and $\langle R_{g_\perp}{}^2 \rangle / N^{2\nu}$ (b, bottom) vs the crossover scaling variable $|\Delta| N^{\phi}$ where $\Delta \equiv \epsilon/\epsilon_c - 1$. Different symbols show various chain lengths as indicated. The flat branch in each figure refers to $|\epsilon| < |\epsilon_c|$, while the other branch refers to $|\epsilon| > |\epsilon_c|$. Ideally, for large $|\Delta| N^{\phi}$ the increasing branch in part a and the decreasing branch in part b should tend to straight lines, the slope of which would yield the theoretical exponents expected for large $|\Delta| N^{\phi}$, $2(\nu_2 - \nu)/\phi \approx 0.55$ and $-2\nu/\phi \approx -2.03$, respectively.

not involve any critical exponents different from $\nu = 0.59$ but involves only the prefactors in the power laws, eq 8.

4. Chain Dynamics near the Adsorption Transition

We start by briefly reviewing what is known about the chain relaxation of our model in the bulk. In previous work, it has been demonstrated[25,26] that this model of polymer chains in dilute solution in the bulk reproduces all the properties expected for the Rouse dynamics in the presence of excluded volume interactions:[41] the relaxation time scales as

$$\tau_N \approx W^{-1} N^z \qquad z = 2\nu + 1 \approx 2.18 \tag{10}$$

where W is a rate for the reorientation of effective monomeric units. The diffusion constant D_N simply scales inversely with the chain length,

$$D_N \propto \langle l^2 \rangle W/N \tag{11}$$

where a prefactor of order unity is ignored. The power law eq 10 then simply can be understood from the scaling argument, that the chain diffuses a distance of

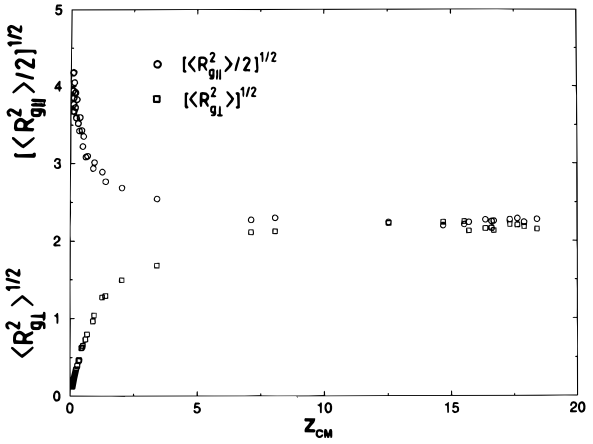

Figure 9. Plot of the root mean square gyration radii components, $[\langle R_{g\parallel}{}^2\rangle/2]^{1/2}$ and $\langle R_{g\perp}{}^2\rangle^{1/2}$, versus the center of mass position of the chain Z_{CM}, for $N = 32$ and $\epsilon = -1.0$.

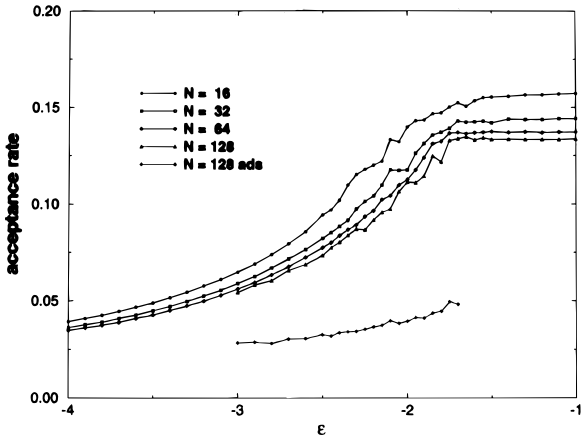

Figure 10. Acceptance rate A plotted vs ϵ for four different chain lengths. Note that shorter chains have a somewhat higher acceptance rate due to higher mobility of monomers at the chain ends. For inner monomers of a free chain off the wall the acceptance rate is about 0.13, while for monomers forming trains adsorbed at the surface it is about 0.03. For $N = 128$, the acceptance rate for moves of monomers which sit within the range δ of the adsorption potential is also shown.

the order of its own size during the time τ_N: $D_N\tau_N \propto \langle R_g{}^2\rangle \propto \langle l^2\rangle N^{2\nu}$ yields eq 10, invoking that D_N scales inversely with molecular weight (eq 11). For times t smaller than the chain relaxation time, inner monomers exhibit anomalous diffusion[42] (i.e., a mean-square displacement increasing slower than linear with time)

$$g_1(t) \equiv \langle[\vec{r}_i(t) - \vec{r}_i(0)]^2\rangle \propto \langle l^2\rangle (Wt)^{x_1},$$
$$x_1 = (1 + 1/2\nu)^{-1} \approx 0.54 \quad (12)$$

The physical interpretation of this anomalous diffusion of inner monomers, of course, is that due to the binding of a monomer to its neighbors it cannot diffuse freely but has to "drag" his neighboring monomers with it, and the "effective mass" of this diffusing object in a sense increases with time. Note that the center of mass mean-square displacement does not show any anomalous diffusion at all,

$$g_3(t) \equiv \langle[\vec{r}_{CM}(t) - \vec{r}_{CM}(0)]^2\rangle = 6D_N t \quad (13)$$

It is obvious that for $t \propto \tau_N$ both $g_3(t)$ and $g_1(t)$ match and are of the same order as the mean-square gyration radius,

$$g_1(\tau_N) \propto g_3(\tau_N) \propto \langle l^2\rangle N^{2\nu} \quad (14)$$

Thus, at $t \approx \tau_N$, $g_1(t)$ smoothly crosses over from the anomalous diffusion, described by eq 12, to ordinary diffusion, $g_1(t) = 6D_N t$ {$=g_3(t)$, of course}. It then is useful to consider also a mean-square displacement of inner monomers in the center of gravity system of each chain,

$$g_2(t) = \langle[\vec{r}_i(t) - \vec{r}_{CM}(t) - (\vec{r}_i(0) - \vec{r}_{CM}(0))]^2\rangle \quad (15)$$

While $g_1(t) = g_2(t)$ for $t \ll \tau_N$, one observes a saturation of $g_2(t)$ at large times,

$$g_2(t) \approx \langle R_g{}^2\rangle, \quad t \gg \tau_N \quad (16)$$

We are now interested in understanding how this behavior is modified if the chain is constrained by the wall and the associated binding potential, eq 4. First of all, it is important to note that under the conditions considered in the present work glasslike freezing in of the adsorbed chains is not a problem: the mobility of monomers even in the strongly adsorbed case is still rather large and hence allows lateral diffusion. This fact already becomes evident from a consideration of the acceptance rate A of the attempted Monte Carlo moves (Figure 10). One sees that shorter chains have a higher acceptance rate than long ones, due to end effects, and that the acceptance rate also decreases in a pronounced way at the adsorption transition. However, when we consider the acceptance rate of monomers which are already adsorbed, we notice rather little variation with ϵ: Basically the decrease of A with increasing $|\epsilon|$ for $|\epsilon| \gtrsim |\epsilon_c|$ is due to the fact that more and more monomers become attached to the wall, and no longer belong to the fraction of "free" monomers with high mobility, but to the fraction of adsorbed monomers with low mobility. But, the latter still have a reasonably large acceptance rate, due to moves in directions parallel to the adsorbing walls, such that the monomers do not leave the range of the adsorption potential.

In the presence of the adsorbing wall it is still useful to discuss the chain motions in terms of the displacements g_1, g_2, and g_3, but it now becomes necessary to split these motions into a "longitudinal" part parallel to the surface and a "transverse" part perpendicular to it. Figures 11−14 contain our resulting data for a variety of typical cases, which now shall be discussed. The longitudinal (transverse) displacements are henceforth labeled by an additional index $l(t)$, respectively.

For the shortest chain length ($N = 16$), τ_N is too small to allow a well-developed regime where the anomalous diffusion as described by eq 12 could be seen. In fact, there is always a distinction visible between $g_1(t)$ and $g_2(t)$, even at very early times where the displacement is still small in comparison with the bond length. Also one can see that such short chains are still free at $\epsilon = -2.5$, where long chains already would be adsorbed, as the behavior of the transverse center of mass displacement shows. In contrast, for $\epsilon = -3$ this displacement g_{3t} saturates at a very small value, and also g_{1t}, g_{2t} are hardly distinct from each other and saturate at a small value, too. This behavior is characteristic for an adsorbed chain. Only the longitudinal displacements $\{g_{1l}(t), g_{3l}(t)\}$ increase proportional to the time in all cases shown, indicating that lateral diffusion takes place. The extremely small transverse mean-square displacement of the center of gravity for $\epsilon = -3$ explains why there is practically no distinction between $g_{1t}(t)$ and $g_{2t}(t)$ in this case: the center of mass is tightly bound to the adsorbing wall. While, in the case $\epsilon = -1.5$, both

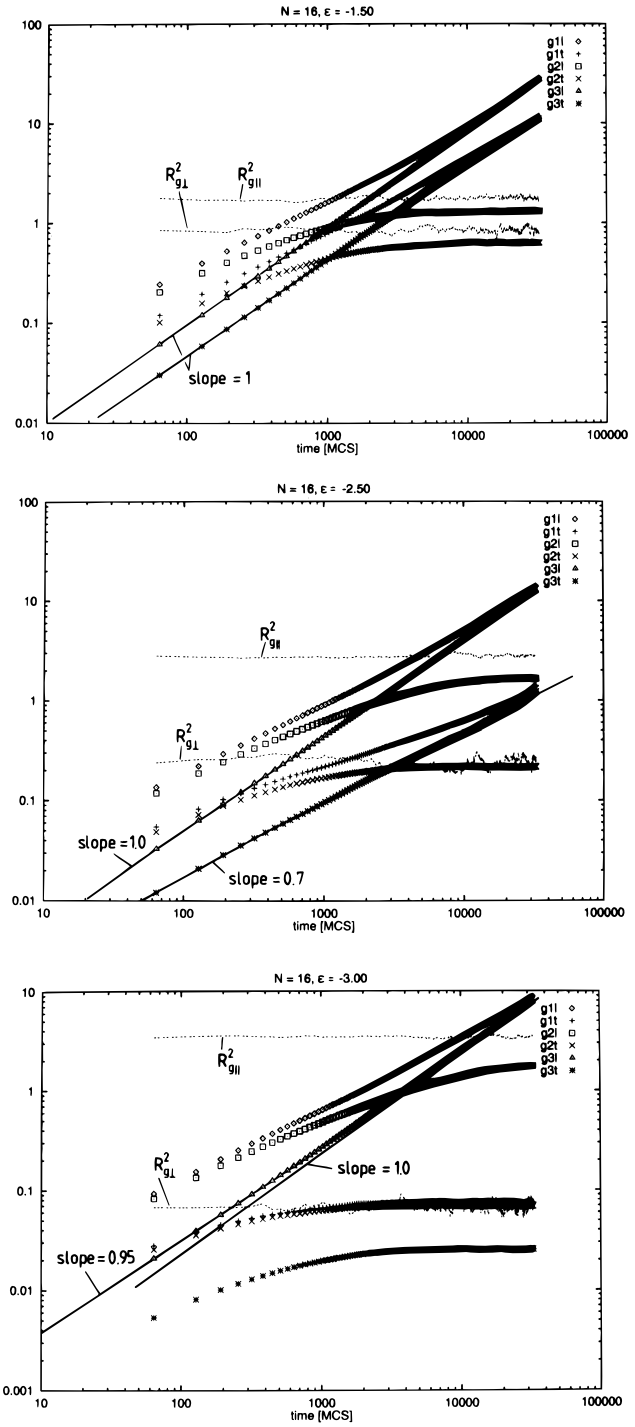

Figure 11. log−log plot of mean-square displacements $g_{1l}(t)$, $g_{1t}(t)$, $g_{2l}(t)$, $g_{2t}(t)$, $g_{3l}(t)$, and $g_{3t}(t)$ plotted vs time for $N = 16$, with adsorption energies $\epsilon = -1.5$ (a, top), -2.5 (b, middle), and -3.0 (c, bottom). Time is measured in attempted Monte Carlo steps per monomer. Fluctuating broken lines indicate the average values of the parallel ($R_{g\parallel}{}^2$) and perpendicular ($R_{g\perp}{}^2$) components of the mean-square gyration radius, depending on how many times the instantaneous position (time interval) may be sampled during the total length of the run. Straight lines indicate power laws with effective exponents as indicated.

$g_{3l}(t) \propto t$ and $g_{3t}(t) \propto t$ over the full range of time shown, for $\epsilon = -2.5$ one observes $g_{3t}(t) \propto t^{x_{3t}}$ with $x_{3t} \approx 0.7$, for more than 2 decades of time. This anomalous behavior clearly is due to the vicinity of the adsorption transition. For $\epsilon = -3$ we see a slightly anomalous behavior also for the longitudinal part, $g_{3l}(t) \propto t^{x_{3l}}$ with $x_{3l} \approx 0.95$ for $100 \lesssim t \lesssim 10000$.

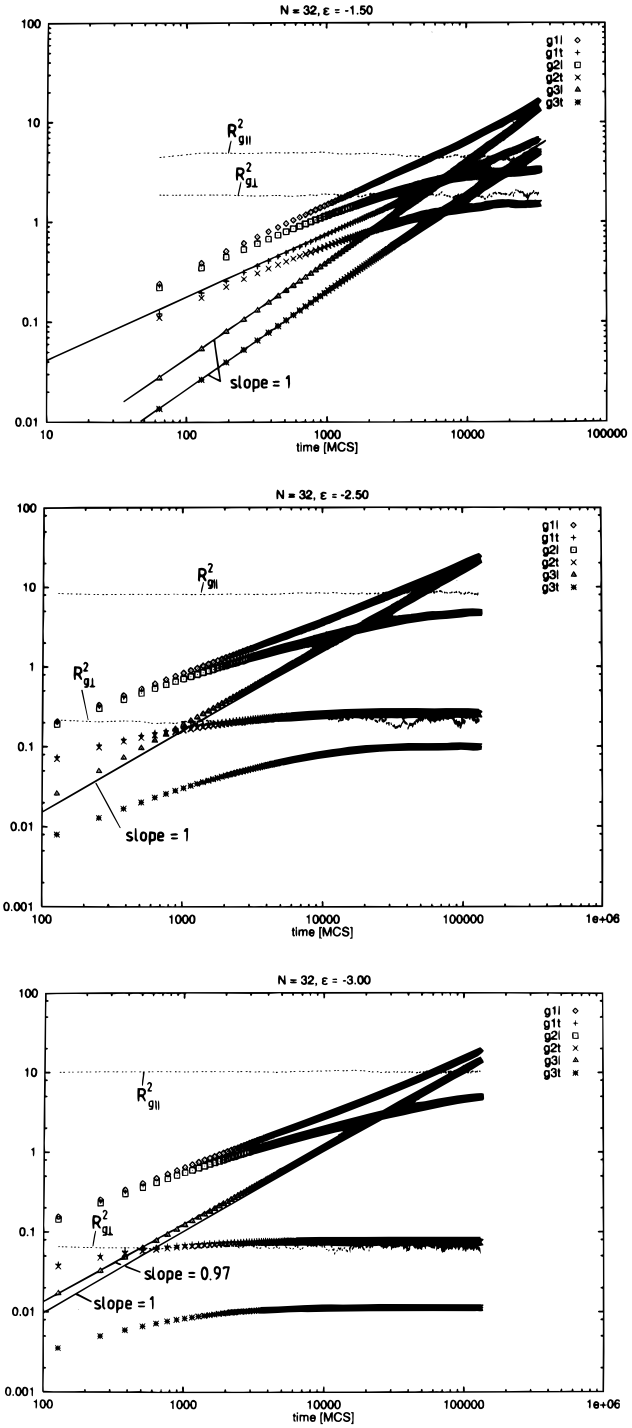

Figure 12. Same as Figure 11 but for $N = 32$.

For the somewhat longer chains ($N = 32$, 64) the behavior is still similar in the nonadsorbed case: both $g_{3l}(t)$ and $g_{3t}(t)$ increase linearly with time. But now for $\epsilon = -2.5$ the transverse displacements saturate already; a chain of length $N = 32$ is already tightly bound to the wall. Again $g_{3l}(t) \propto t^{x_{3l}}$, with $x_{3l} \approx 0.97$ similar to that discussed above. Data for $N = 64$ were also recorded but are qualitatively similar to those for $N = 32$ and hence are not shown here. For the case $N = 128$, $\epsilon = -1.5$, we have also included the slopes of g_{1t} and g_{1l}. These data would imply $x_1 \approx 0.6$, but we note that a distinctly smaller value would result if we would fit a power law to the initial part of the corresponding data for $g_{1l}(t)$ and $g_{1t}(t)$, respectively ($x_1 \approx 0.53$). Thus, the data are roughly consistent with the expectations noted above (eq 12). Within our accuracy, for $N = 128$ the data for the longitudinal displacement $g_{3l}(t)$ are compat-

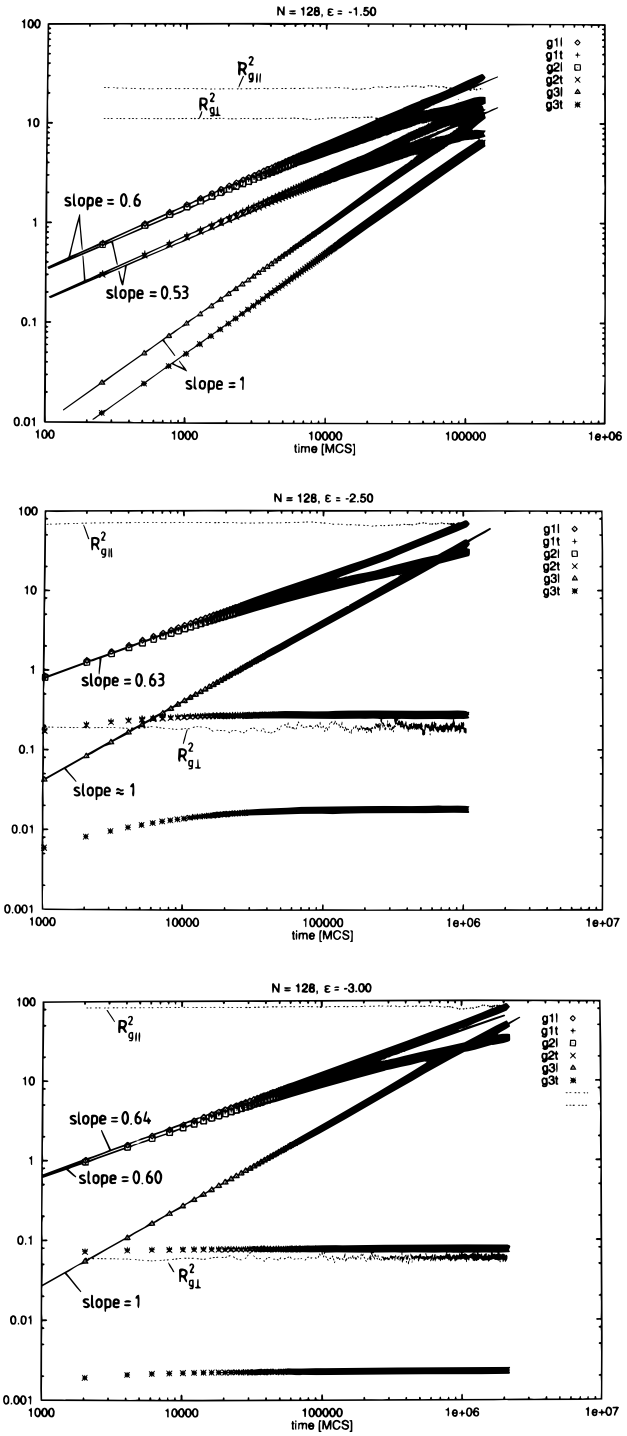

Figure 13. Same as Figure 11 but for $N = 128$.

ible with normal diffusion, eq 13, while $g_1(t) \propto t^{x_1^{\text{eff}}}$ with $x_1^{\text{eff}} \approx 0.62 \pm 0.02$. This is again slightly larger than the expected value (note that $\nu = {}^3/_4$ in $d = 2$ dimensions implies $x_1 = (1 + 1/2\nu)^{-1} = {}^3/_5$). The fact that for these long chains the mean-square displacement parallel to the adsorbing wall exhibits nice ordinary diffusion, $g_{3l}(t) \propto t$ for all times and all ϵ indicates that the different behavior of the shorter chains simply is a kind of "finite size rounding" effect of the adsorption transition at $\epsilon = \epsilon_c$: As emphasized already in the above discussion of static properties, for finite chain length N the singular behavior at the adsorption transition is smeared out over a regime $|\Delta| \propto N^{-\phi}$, where $\Delta = \epsilon/\epsilon_c - 1$ and ϕ is the crossover exponent. Right at the adsorption transition, i.e., in the limit $\Delta \to 0$, $N \to \infty$, we do expect anomalous diffusion $g_{3t}(t) \propto t^{x_{3t}}$, $g_{3l}(t) \propto t^{x_{3l}}$, where these exponents

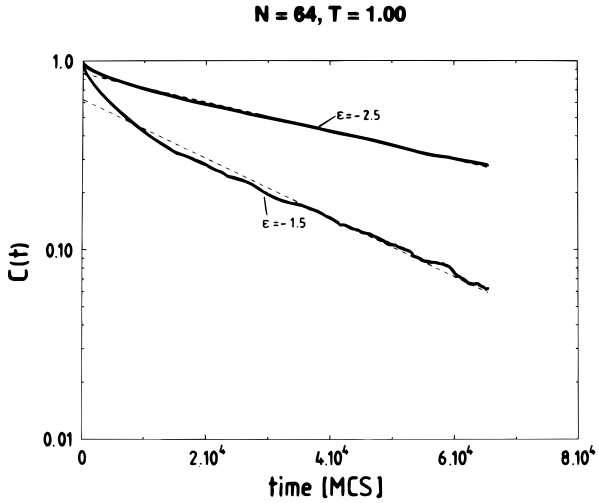

Figure 14. Semilog plot of the end-to-end correlation function $C(t)$ (eq 17) vs time t, for chain length $N = 64$ and two choices of ϵ. Dashed straight lines indicate possible fits to a behavior $C(t) \propto \exp(-t/\tau)$.

x_{3l}, x_{3t} have well-defined and nontrivial values. This anomalous behavior is related to the fact that $x_{3t} = 1$ in the nonadsorbed case, while $x_{3t} = 0$ in the adsorbed case (g_{3t} settles down at a finite displacement). This anomalous diffusion for $\Delta = 0$ is similar to anomalous diffusion at other critical points[43] (or to diffusion of point particles at percolation clusters,[44] etc.). Since right at the adsorption transition the adsorbed chains can have loops on all length scales up to the coil size, the motion is neither of two-dimensional nor of three-dimensional character, and this special structure between dimensionalities is responsible for the anomalous diffusion here. For finite N and $|\Delta|$ nonzero the data still are slightly affected by crossover between normal diffusion (which prevails for $|\Delta| > 0$ in the limit $N \to \infty$) and anomalous diffusion (which prevails for $\Delta = 0$ in the limit $N \to \infty$). Consistent with this interpretation, anomalous diffusion is the more pronounced the shorter the chains are.

We now characterize the relaxation of the chains by various relaxation times. A standard method to do this considers the time-displaced correlation function of the end-to-end vector of the chain,[28,29]

$$C(t) = \langle \vec{R}(0) \cdot \vec{R}(t) \rangle / \langle \vec{R}^2 \rangle \tag{17}$$

and since one expects $C(t) \propto \exp(-t/\tau)$ for large enough times, one can extract a relaxation time τ from a semilog plot of $C(t)$ vs time (Figure 14). Unfortunately, strong statistical fluctuations make it somewhat ambiguous to extract a time τ in this way: the exponential decay law does not hold at shorter times, and it is not easy to disentangle from the statistical noise these systematic deviations from a single-exponential decay (a whole spectrum of relaxation times contributes). Therefore we have followed previous practice[25,26,30,45] to define relaxation times from the mean-square displacements, using suitable intersections: i.e., a time τ_3^l for the longitudinal relaxation (displacements parallel to the adsorbing wall) is defined in[30]

$$g_{3l}(t = \tau_3^l) = {}^2/_3 \langle {R_{g_\perp}}^2 \rangle \tag{18}$$

Note that the factor ${}^2/_3$ in this definition is an arbitrary convention, simply used for consistency with previous work[30,45] {the more natural choice $g_{3l}(t = \tilde{\tau}_3^l) = \langle {R_{g_\parallel}}^2 \rangle$ is not used because often this requires enormous effort in

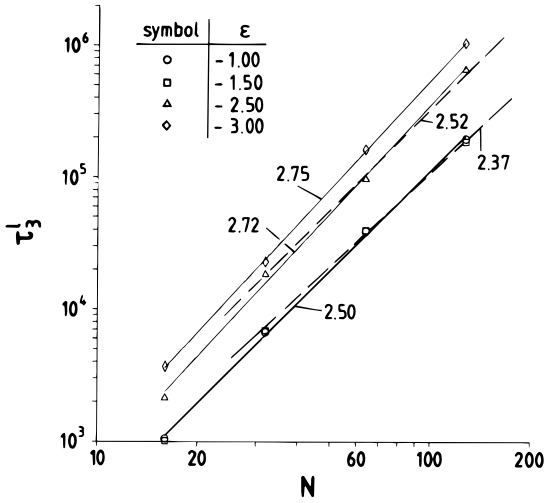

Figure 15. log−log plot of the relaxation time τ_3^1 (eq 18) vs chain length N, for four values of ϵ, as indicated. Full straight lines indicate power law fits including the shortest chain length $N = 16$, while broken lines indicate power law fits where $N = 16$ is excluded. Effective exponents z_{eff} are quoted.

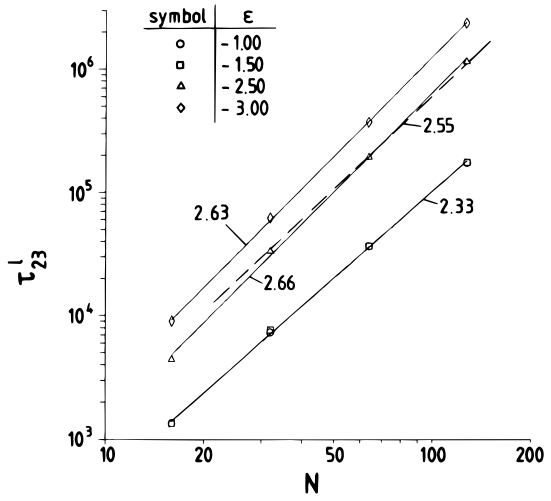

Figure 16. Same as Figure 15, but for τ_{23}^1 (eq 19).

computing time—e.g., in Figure 13c the time $\tilde{\tau}_3^1$ would still be outside the range of the data points—and one believes that τ_3^1 and $\tilde{\tau}_3^1$ differ only by a numerical factor}. Another time defined from such an intersection condition, that can be easily read off from the graphs Figures 11−13, is the time τ_{23}^1 [30]

$$g_{2l}(t = \tau_{23}^1) = g_{3l}(t = \tau_{23}^1) \tag{19}$$

Figures 15 and 16 show log−log plots of these times versus chain length for several choices of ϵ. In the asymptotic limit of very long chains, we expect a power law as written in eq 10 with $z \approx 2.18$, for all values of ϵ in the nonadsorbed regime, while in the adsorbed case ($|\epsilon| > |\epsilon_c|$) a similar law with two-dimensional exponents should hold

$$\tau_N \propto N^{z_2}, \quad z_2 = 2\nu_2 + 1 = 2.5, \quad N \to \infty \tag{20}$$

From Figures 15 and 16 we see that the data indicate an increase of the (effective) exponent z_{eff} in the power laws $\tau_3^1 \propto N^{z_{eff}}$, $\tau_{23}^1 \propto N^{z_{eff}}$, when one compares the behavior of the adsorbed chains ($|\epsilon| > |\epsilon_c|$) with the nonadsorbed ones: but the effective exponents for τ_3^1 and τ_{23}^1 are not in exact agreement with each other (as they should, for long enough chains), and they also are somewhat larger than the theoretical predictions, eqs 10 and 20. However, it is apparent (particularly for the data at $\epsilon = -2.50$, where the chain length $N = 16$ still behaves as effectively nonadsorbed, cf. Figure 11) that the discrepancy between simulation and theoretical prediction gets smaller when the shortest chain length ($N = 16$) is excluded from the power law fit. We consider it likely that due to a slight curvature (which is hard to see on Figures 15 and 16, since these plots span only 1 decade in N, but it may be spread out over several decades) for $N \to \infty$ the expected behavior indeed will be recovered. The reason for the apparent enhancement seen here again is the crossover to a slower relaxation at the adsorption transition. Since we have argued already that for $\Delta = 0$ anomalous diffusion occurs, simple scaling arguments imply that $\tau_N(\Delta = 0) \propto N^{z_c}$ with $z_c > z$: Assuming that τ_N can be characterized by the condition that $g_{3t}(t) \approx \langle R_{g_\perp}{}^2 \rangle$ and noting that $\langle R_{g_\perp}{}^2 \rangle \propto N^{2\nu}$ even for $\Delta = 0$, we conclude with $g_{3t}(t) \approx (W_3 t)^{x_3}$

$$g_{3t}(t = \tau_N) = (W_3 \tau_N)^{x_3} \approx \langle R_{g_\perp} \rangle \propto N^{2\nu} \tag{21}$$

Now the chain length dependence of the rate W_3, $W_3 \propto N^{-w}$, is estimated from the condition that at $t = 1$ the finiteness of the acceptance rate (Figure 10) should lead to a mean-square displacement of the center of gravity of order $1/N$: at short times the monomer displacements add up independently and randomly, and each monomer displacement of order unity produces a mean-square displacement or order N^{-2} of the center of gravity, and the time unit is such that there are N attempted monomer motions per unit time. This yields $wx_3 = 1$, i.e., $w = 1/x_3$. Using now for $\Delta = 0$ $\tau_N \propto N^{z_c}$, eq 21 yields

$$N^{-1+x_3 x_c} = N^{2\nu}, \quad z_c = (2\nu + 1)/x_3 \tag{22}$$

Thus, anomalous diffusion ($x_3 < 1$) implies $z_c > 2\nu + 1$. Since at $t = \tau_N$ also a smooth crossover to ordinary diffusion $\{g_{3t}(t > \tau_N) = D_N t\}$ should occur, we also can estimate the diffusion constant,

$$D_N \propto \langle R_{g_\perp}{}^2 \rangle / \tau_N \propto N^{-y_c}, \; y_c = [2\nu(1 - x_3) + 1]/x_3 > 1 \tag{23}$$

Unfortunately, the present computer resources do not yet allow a meaningful estimation of the relaxation time at the adsorption transition itself (it is difficult to locate it precisely for our model, and the relaxation is very slow and sluggish there), and hence we do not give any estimates for the exponents x_3, y_c, and z_c here.

But it is of interest to study directly from the simulation the diffusion constant for lateral motion, parallel to the wall, since this quantity is well-defined for adsorbed chains also (Figure 17). The resulting effective exponents all exceed the Rouse behavior ($y = 1$) slightly, but again slight curvature is present on this log−log plot, and it is expected that a $D_l \propto N^{-1}$ behavior does indeed result for large enough N.

Finally we consider the dependence of the diffusion constant D_l and the relaxation time τ_3 on ϵ (Figures 18 and 19). As expected already from Figure 17, $D_l(\epsilon)$ is independent of ϵ for $|\epsilon| < |\epsilon_c|$: this is expected, since chains in the nonadsorbed phase are not constrained to be close to the surface, and we simply see the free diffusion of a bulk chain. In the adsorbed phase, the diffusion constant decreases smoothly. This decrease is approximately proportional to the fraction of adsorbed monomers. Our data do not give any evidence for a glassy behavior of strongly adsorbed chains for large ϵ,

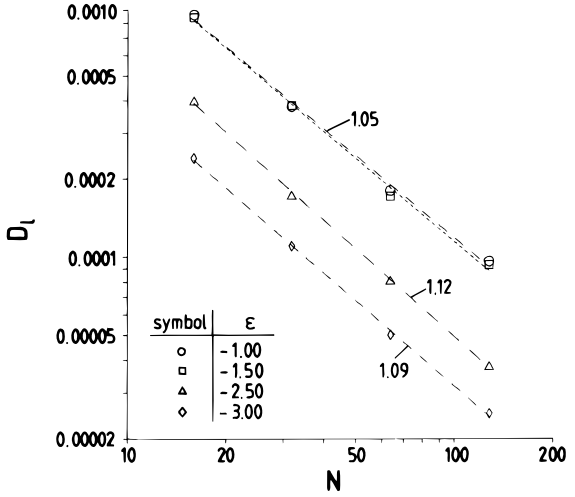

Figure 17. log−log plot of the longitudinal diffusion constant D_l vs chain length N, for four values of ϵ as indicated. Broken straight lines show fits to power laws $D_l \propto N^{-y_{eff}}$, and the numbers quoted show the resulting effective exponents y_{eff}.

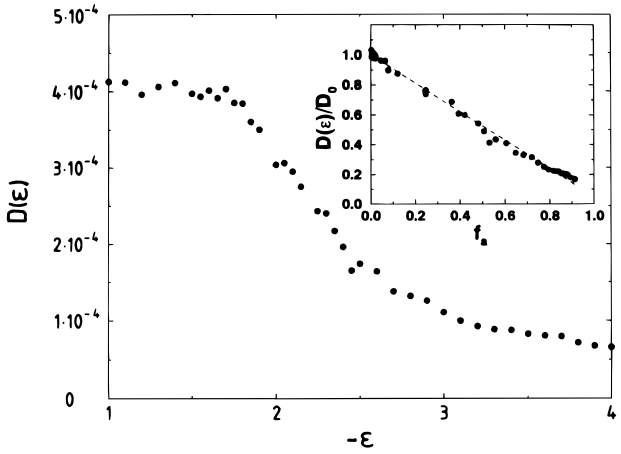

Figure 18. Lateral diffusion constant $D_l(\epsilon)$ plotted vs $|\epsilon|$ for $N = 32$. Insert shows the same data replotted vs the fraction f_a of adsorbed monomers.

at least not for such short chains {$D_l(\epsilon)$ does not extrapolate to zero even for $f_a \to 1$!}. The data for τ_{3l} indicate also a very smooth variation with ϵ. In particular, no evidence for a critical anomaly as $|\epsilon| \to |\epsilon_c|$ is seen {such an evidence could occur only in the regime $|\epsilon| > |\epsilon_c|$, since for nonadsorbed chains the behavior is again dominated by chains in the bulk solution}. Since the straight line shown in Figure 19 represents a law $\tau_3^l = \tau_3^l(\epsilon = \epsilon_c) \exp(\epsilon_c - \epsilon)$, we also see no significant deviation from simple thermally activated behavior. But one must admit that the data in Figure 19 are rather noisy and the chain length $N = 32$ may be too short to give clear evidence for anomalous effects associated with the adsorption transition and a (possible) glass transition (at large $|\epsilon|$, if one occurs). Here we recall that a simple thermally activated behavior of the same model has also been found for the motion of chains confined to pores with attractive walls.[30] Of course, the simple behavior of Figure 19 may be related to the fact that our substrate surface is ideally flat and nonrough, and lateral motion is so easily possible. Real surfaces that are rough may well behave differently, but it also is conceivable that the characteristics of the glass transition then are linked to the nature of this roughness.

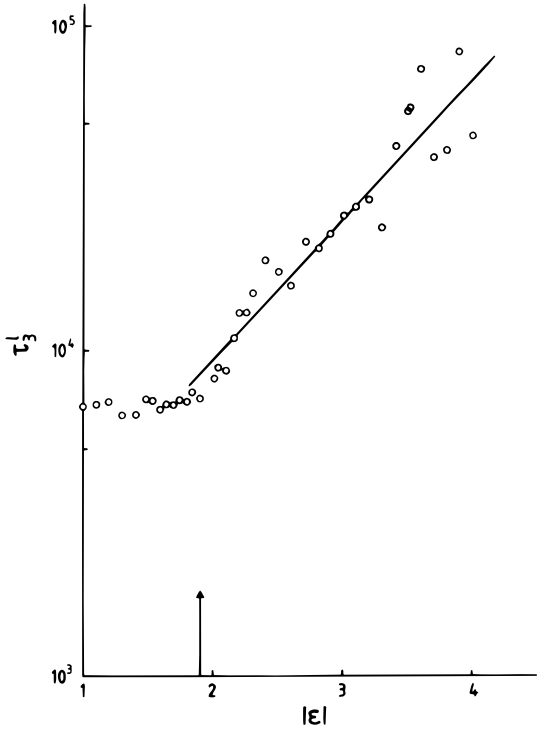

Figure 19. Semilog plot of τ_3^l vs $|\epsilon|$ for $N = 32$. Straight line shows an Arrhenius-like behavior. Arrow shows the location of the adsorption transition.

5. Conclusions

In this paper, the dynamical behavior of chains exposed to a repulsive wall with a short-range attractive wall potential of varying strength has been considered. As a first step, the adsorption transition—where a chain near the wall changes from a quasi-two-dimensional configuration to a three-dimensional one—has been located, analyzing the monomer density distribution as a function of the distance from the wall, the total internal energy of the chain, the fraction of monomers located within the range of the adsorption potential, etc. An investigation of the acceptance rate of the attempted monomer moves shows that the adsorbed polymer chains are not frozen in; even for values of $|\epsilon|$ exceeding the adsorption threshold $|\epsilon_c|$ by more than a factor of 2, there is still a reasonably high mobility. This is rather remarkable, since for typical cases such as $N = 128$, $\epsilon = -3$, where $\langle R_{g\parallel}^2 \rangle \approx 80$, $\langle R_{g\perp}^2 \rangle \approx 0.06$ (cf. Figure 13c), the available volume (in units of length defined by $l_{max} = 1$, cf. eq 1) for a chain is of the order of $V \approx \langle R_{g\perp}^2 \rangle^{1/2} (\pi \langle R_{g\parallel}^2 \rangle) \approx 61.6$; i.e., the density $\phi = N/V \approx 2.08$ exceeds melt densities,[25,26] which have been estimated as about $\phi \approx 1.5$. In the present case, relaxation at this high density is still possible due to components of the motion in the third dimension (perpendicular to the adsorbing surface) and at the (one-dimensional) free boundary of the (two-dimensional) coil.

Of course, it is interesting to compare our study to simulations of chains which have been restricted to two dimensions from the outset. Such a study is available in the framework of the bond fluctuation model.[46] In that work, evidence was presented for a simple Rouse-like relaxation, where (in the presence of excluded volume) one has $\langle R_g^2 \rangle \propto N^{2\nu}$ with $\nu = 3/4$ and the diffusion constant still scales inversely with the molecular weight, $D_N \propto 1/N$ (i.e., the exponent $y \equiv 1$). Also evidence for the anomalous diffusion of monomer ($g_1 \propto t^{x_1}$ with $x_1 = 0.6$) was presented.

The present model behaves similar to such a strictly two-dimensional model for the longest chain length ($N = 128$), while for shorter chains deviations occur. We find a somewhat too large value of the exponent of the relaxation time, $z \approx 2.65 \pm 0.10$, instead of the theoretical expected value $z = 2\nu_2 + 1 = 2.5$. Also the decrease of the diffusivity is somewhat too rapid ($D_1 \propto N^{-y}$ with $y \approx 1.05$), and the exponent $x_1 \approx 0.65$, while $x_1 \approx 0.6$ already in the nonadsorbed regime. However, these discrepancies can be interpreted in terms of crossover problems associated with the adsorption transition, which leads to critical phenomena in the limit $N \rightarrow \infty$, $|\epsilon| \rightarrow |\epsilon_c|$.

By an analysis of the dependence of the diffusivity and relaxation time on $|\epsilon|$ it was found that these quantities vary rather monotonically; they show a kinklike decrease (or increase, respectively) at $|\epsilon_c|$, and an Arrhenius-like variation at large $|\epsilon|$.

Throughout the range studied here, a glassy freezing does not occur. However, one should be cautious in carrying over this conclusion to experiments: the present study concerns both very flexible, very short chains and an ideal, structureless substrate. For adsorption of either stiffer chains and/or rough irregular substrates, as it will occur for real materials, a differing conclusion is conceivable. Also the scaling relations for relaxation times cannot immediately be carried over to experiment, since hydrodynamic interactions (present in real solutions) are not included for our model. It is not clear to what extent hydrodynamic forces affect the motions of strongly adsorbed chains, however.

There are many directions in which an extension of the present research can be envisaged: here we have only considered single chains, implying an extremely dilute solution in a very good solvent. However, the present model can easily deal with solvents of variable quality and higher concentrations.[26] Clearly it is interesting to study kinetics of adsorbed chains under these different circumstances. It is also possible to study the confinement of chains between two parallel walls—results for this case will be presented shortly.[47]

Finally it is of great interest to study adsorbed films of finite thickness, with another interface against the solvent (or vacuum, respectively). A further interesting extension would be to add solvent molecules explicitly, carrying out a molecular dynamics simulation to incorporate the effects of hydrodynamic interactions, describing hence chain dynamics in the framework of the Zimm model[41,48] rather than the Rouse model.[41] Such studies of chains in dilute solution in the bulk have become feasible recently,[49,50] but the extension to chains near walls remains to be done. We hope that the present research will also stimulate further experiments and contribute toward their correct interpretation.

Acknowledgment. This research has been supported by the Deutsche Forschungsgemeinschaft (DFG) under Grant No. 435-BUL-113/45 and by the Bulgarian Ministry for Science and Education under Grant No. X-301/93. We are grateful to I. Gerroff and W. Paul for fruitful interactions in the early stages of this project.

References and Notes

(1) Sanchez, I. C., Ed. *Physics of Polymer Surfaces and Interfaces*; Butterworth-Heinemann: Boston, 1992.
(2) Wu, S. *Polymer Interfaces and Adhesion*; Dekker: New York, 1982.
(3) Fleer, G. J.; Cohen Stuart, M. A.; Scheutjens, J. M. H. M.; Cosgrove, T.; Vincent, B. *Polymers at Interfaces*; Chapman & Hall: London, 1993.
(4) Tirrell, M.; Parsonage, E. E. Structure and Properties of Polymers. In *Materials Science and Technology*; Thomas, E. L., Ed.; VCH: Weinheim, 1993; Vol. 12, p 653.
(5) Eisenriegler, E. *Polymers near Surfaces*; World Scientific: Singapore, 1993.
(6) Granick, S. In ref 1; p 227. Semenov, A. N.; Joanny, J. F. *J. Phys. II* (*Fr.*) **1995**, *5*, 859.
(7) Yu, H. In ref 1; p 263.
(8) Kremer, K. *J. Phys.* (*Paris*) **1986**, *47*, 1269.
(9) Chakraborty, A. K.; Adriani, P. M. *Macromolecules* **1992**, *25*, 2470.
(10) Bitsanis, I.; Hadziioannou, G. *J. Chem. Phys.* **1990**, *92*, 3827.
(11) Chakraborty, A. K.; Shaffer, J. S.; Adriani, P. M. *Macromolecules* **1991**, *24*, 5226.
(12) Lai, P. Y. *Phys. Rev. E* **1994**, *49*, 5420.
(13) Halperin, A.; Tirrell, M.; Lodge, T. P. *Adv. Polym. Sci.* **1991**, *100*, 31.
(14) Milner, S. T. *Science* **1991**, *100*, 31.
(15) Grest, G. S.; Murat, M. In *Monte Carlo and Molecular Dynamics Simulations in Polymer Science*; Binder, K., Ed.; Oxford University Press: Oxford, U.K., 1995; Chapter 9.
(16) Binder, K.; Lai, P. Y.; Wittmer, J. *Faraday Discuss.* **1994**, *98*, 97.
(17) Mansfield, K. F.; Theodorou, D. N. *Macromolecules* **1991**, *24*, 6283.
(18) Bitsanis, I. A.; ten Brinke, G. *J. Chem. Phys.* **1993**, *99*, 3100.
(19) Kumar, S. K.; Vacatello, M.; Yoon, D. Y. *Macromolecules* **1990**, *23*, 2189.
(20) Winkler, R. G.; Matsuda, T.; Yoon, D. Y. *J. Chem. Phys.* **1993**, *98*, 729.
(21) De Gennes, P. G. *C. R. Acad. Sci., Ser. 2* **1985**, *301*, 1399.
(22) De Gennes, P. G. *C. R. Acad. Sci., Ser. 2* **1986**, *302*, 765.
(23) Binder, K. *Progr. Colloid Polym. Sci.* **1994**, *96*, 7.
(24) Paul, W.; Baschnagel, J. In *Monte Carlo and Molecular Dynamics Simulations in Polymer Science*; Binder, K., Ed.; Oxford University Press: Oxford, U.K., 1995; Chapter 6.
(25) Gerroff, I.; Milchev, A.; Binder, K.; Paul, W. *J. Chem. Phys.* **1993**, *98*, 6526.
(26) Milchev, A.; Paul, W.; Binder, K. *J. Chem. Phys.* **1993**, *99*, 4786.
(27) Milchev, A.; Binder, K. *Macromol. Theory Simul.* **1994**, *3*, 915.
(28) Kremer, K.; Binder, K. *Comput. Phys. Rep.* **1988**, *8*, 259.
(29) Sokal, A. In *Monte Carlo and Molecular Dynamics Simulations in Polymer Science*; Binder, K., Ed.; Oxford University Press: Oxford, U.K., 1995; Chapter 2.
(30) Milchev, A.; Paul, W.; Binder, K. *Macromol. Theory Simul.* **1994**, *3*, 305.
(31) De Gennes, P. G. *Scaling Concepts in Polymer Physics*; Cornell University Press: Ithaca, NY, 1979.
(32) Eisenriegler, E.; Kremer, K.; Binder, K. *J. Chem. Phys.* **1982**, *77*, 6296.
(33) Livne, S.; Meirovitch, H. *J. Chem. Phys.* **1988**, *88*, 4494.
(34) Meirovitch, H.; Livne, S. *J. Chem. Phys.* **1988**, *88*, 4507.
(35) Van Dieren, F.; Kremer, K. *Europhys. Lett.* **1987**, *4*, 569.
(36) Balazs, A. C.; Huang, K.; McElwain, P. *Macromolecules* **1991**, *24*, 714. Van der Linden, C. C.; Van Lent, B.; Leermakers, F. A. M.; Fleer, G. J. *Macromolecules* **1994**, *27*, 1915.
(37) Haas, F. M.; Hilfer, R.; Binder, K. *J. Chem. Phys.* **1995**, *102*, 2960.
(38) We are indebted to O. V. Borisov for a helpful discussion on this point.
(39) Baumgärtner, A.; Binder, K. *J. Chem. Phys.* **1981**, *75*, 2994.
(40) Diehl, H. W.; Dietrich, S. *Z. Phys.* **1981**, *B42*, 65.
(41) Doi, M.; Edwards, S. F. *The Theory of Polymer Dynamics*; Clarendon Press: Oxford, U.K., 1986.
(42) Kremer, K.; Binder, K. *J. Chem. Phys.* **1984**, *81*, 6381.
(43) Hohenberg, P. C.; Halperin, B. I. *Rev. Mod. Phys.* **1977**, *49*, 435.
(44) Bunde, A., Havlin, S., Eds. *Fractals and Disordered Systems*; Springer: Berlin, 1991.
(45) Paul, W.; Binder, K.; Heermann, D. W.; Kremer, K. *J. Chem. Phys.* **1991**, *95*, 7726.
(46) Carmesin, I.; Kremer, K. *Macromolecules* **1988**, *21*, 2819.
(47) Milchev, A.; Binder, K. *J. Comput.-Aided Mater. Des.*, in press.
(48) Zimm, B. H. *J. Chem. Phys.* **1956**, *24*, 20.
(49) Dünweg, B.; Kremer, K. *Phys. Rev. Lett.* **1991**, *66*, 2996.
(50) Pierleoni, C.; Ryckaert, J. P. *Phys. Rev. Lett.* **1991**, *66*, 2992.

MA950668B